Pretransitional Effects Near the Hexagonal−Micellar Phase Transition of the $C_{12}EO_6/H_2O$ Lyotropic Mixture

L. Sallen,[†] P. Sotta,*[,‡] and P. Oswald[†]

Laboratoire de Physique, Ecole Normale Supérieure de Lyon, URA 1325 associée du CNRS, 46 Allée d'Italie, 69364 Lyon Cedex 07, France, and Laboratoire de Physique des Solides, Université de Paris-Sud, Bâtiment 510, 91405 Orsay Cedex, France

Received: October 1, 1996; In Final Form: April 16, 1997[⊗]

The transition hexagonal phase/fluid isotropic phase in the nonionic binary system $C_{12}EO_6$/water is studied. The birefringence of a planar monodomain and the water deuterium NMR splitting are measured as functions of the temperature in the hexagonal phase, at the azeotropic concentration. The planar monodomain is obtained by directional solidification. It is shown that important pretransitional effects exist on approaching the transition. These effects are interpreted as due to the appearance of defects which announce the high-temperature isotropic phase. These defects may consist either of a fragmentation of the columns in segments of finite length or of bridges connecting neighboring cylinders. The activation energy associated with these defects is estimated to be of the order of 0.13 eV/surfactant molecule. The mean length between defects along a column at the transition is estimated to be of the order of 80 nm. Finally an estimate is given for the curvature and saddle splay elastic constants of the monolayer.

1. Introduction

Poly(oxyethylene) surfactants such as the $C_{12}EO_6$ (hexaethylene glycol dodecyl ether) are widely used as emulsifying agents and detergents. Like ionic surfactants, they form micelles in water at small concentrations (above the critical micelle concentration (cmc)) and liquid crystal phases (mesophases) at high concentrations. In the $C_{12}EO_6/H_2O$ system, the mesophases observed on increasing the concentration are a hexagonal phase H_α, a bicontinuous cubic phase (V_1), and a lamellar phase L_α.[1]

In all of these phases, the surfactant molecules form aggregates of different shapes and topologies, such as spheres, cylinders, infinite periodic minimal surfaces, or plane bilayers. Understanding how these aggregates transform into each other at the phase transitions has been a challenge of the past 2 decades in this field.

This problem has already received considerable attention at the lamellar−fluid isotropic phase transition.[2−5] It was shown, by using different techniques, that this transition is mediated by defects. For instance, ESR experiments have revealed the existence of regions in the lamellae where the interfacial film is highly curved, [3] while electron microscopy observations have shown the existence of dislocation loops that cross the layers.[4] It was proposed that the cores of these dislocations are related to the defects observed in ESR, but the presence of pores in the lamellae cannot be ruled out. The existence of defects was also confirmed by birefringence and order parameter measurements,[5] as well as by plasticity[6] and rheology[7] experiments.

The cubic−hexagonal phase transition has also been studied by X-ray diffraction in this system. It was shown that precise epitaxial relations exist between these two phases.[8]

In this article, we are interested in the hexagonal−fluid isotropic phase transition. So far, this transition has not been studied in detail. This is largely due to the difficulty in orienting the very viscous hexagonal phase. Indeed, freezing a sample sandwiched betwen two parallel glass plates from the isotropic liquid into the hexagonal phase systematically leads to a fan-shaped texture in which the columns are completely disoriented. Under the same conditions, the lamellar phase spontaneously orients to the homeotropic anchoring, which has made possible most of the above-mentioned experiments at the lamellar−micellar phase transition. Recently, we have developed a new method which allows one to obtain planar monodomains of the hexagonal phase by directional solidification from the micellar phase.[9] In this paper, we take advantage of this new technique to study how the hexagonal phase melts into the fluid isotropic phase. We shall first show that the birefringence varies abnormally when the isotropic phase is approached (section 2). This result is confirmed by order parameter measurements with deuterium NMR. We shall interpret these measurements as being due to the appearance of defects on approaching the transition (section 3). The exact nature of these defects remains to be elucidated, since the structure of the fluid isotropic phase above the hexagonal phase is itself not completely understood.

2. Experimental Results

2.1. Birefringence. We measured the birefringence of the hexagonal phase as a function of the temperature when approaching the isotropic phase. This method was already successfully used to characterize the lamellar−isotropic phase transition in the same system.[5] This latter experiment was made difficult by the existence of a large freezing range at the transition. This required measuring the birefringence locally with a very thin laser beam focused on the regions still lamellar in the coexistence region. To avoid this difficulty and closely approach the phase transition without phase separation, we chose to work at the azeotropic concentration, i.e., at the top of the domain of stability of the hexagonal phase (Figure 1a) (concentration, 50 wt % $C_{12}EO_6$). This is possible in the hexagonal phase, because the transition temperature at the azeotrope is

* Author to whom correspondence should be addressed.
† Ecole Normale Supérieure de Lyon.
‡ Université de Paris-Sud.
⊗ Abstract published in *Advance ACS Abstracts,* June 1, 1997.

S1089-5647(96)03010-6 CCC: $14.00

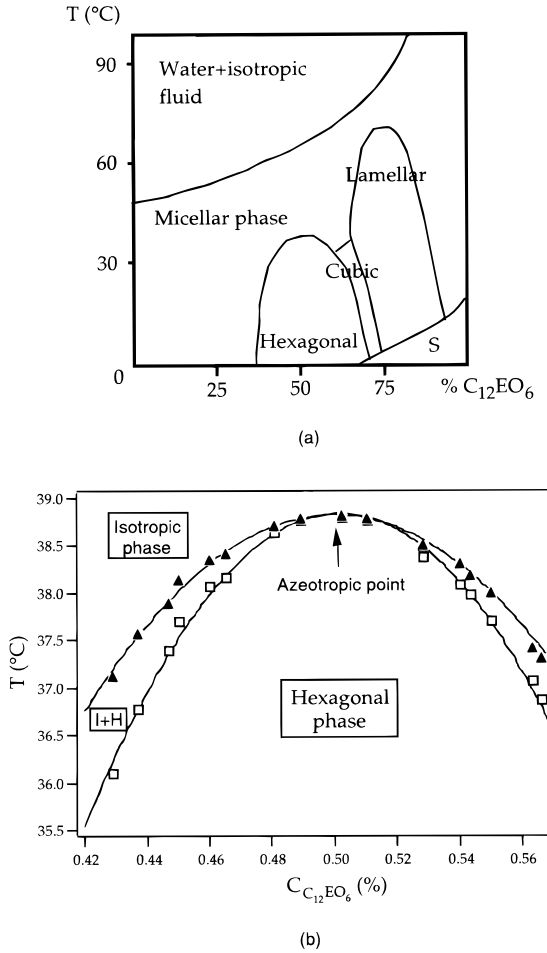

Figure 1. Phase diagram of the $C_{12}EO_6/H_2O$ system: (a) General view (from ref 1); (b) Expansion near the azeotropic point of the hexagonal phase.

not too high, in contrast to the lamellar phase (see the phase diagram in Figure 1a). At this point, the mixture behaves like a pure compound and its freezing range must vanish. In practice, this is verified within 1/100 °C, as shown in the phase diagram in Figure 1b. For precise measurement of the freezing range, the sample is placed in an oven. The temperature is chosen such that the two phases coexist, and then the temperature is slowly decreased (respectively increased), until the isotropic (respectively hexagonal) phase disappears. We allow the system to equilibrate for 20 min between each temperature jump. This procedure is described in detail in ref 10. The uncertainty of the temperatures is estimated to be of the order of 0.02 °C. The very small freezing range which is experimentally measured is due to the presence of residual impurities in the commercial product (from Nikko Ltd.), which we used without further purification.

Our samples are prepared between two parallel glass plates. The thickness is fixed by two spacers made of two nickel wires of diameter 75 μm. The two plates are stuck together on the sides with a photosensitive epoxy glue (Luxtrak LCR 0208 from Epotecny) in which two filling holes are made. This cell is filled by capillarity at 40 °C in a moist atmosphere to avoid evaporation. When the cell is filled, the sample is quickly cooled down in the hexagonal phase and the holes are plugged with the epoxy glue after a rapid cleaning. It is very important to have no bubble in the sample: otherwise, the concentration field is not homogeneous, especially near the bubbles. The samples prepared in this way exhibit a very nice fan-shaped texture, and the birefringence cannot be measured directly. To

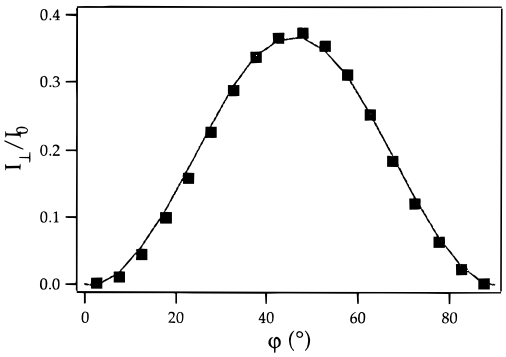

Figure 2. Light intensity $I_\perp$ as a function of φ at $T = 20.73$ °C. The solid line is the best fit to eq 1 and gives $\Delta n \cong 1.55 \times 10^{-3}$.

orient the molecular columns in a single direction and obtain a monodomain in planar orientation, we use directional solidification. This technique and our experimental setup are described in detail in ref 9. Briefly, it consists of growing the hexagonal phase into the isotropic phase at small velocity (typically 1 μm/s) in a temperature gradient of about 30 °C/cm. In this way, we obtain very nice monodomains in planar orientation, with the optical axis perpendicular to the temperature gradient and parallel to the glass plates. We use such samples to measure the birefringence.

The birefringence Δn is obtained by measuring through the microscope the intensity $I_\perp$ of the transmitted light between crossed polarizers as a function of the angle φ between the polarizer and the optical axis. Measurements are performed in Koehler illumination, with the substage iris stopped down as much as possible. This is important for obtaining a parallel beam. Under these conditions, the transmitted intensity is

$$I_\perp = I_0\left(\sin\left(\frac{\pi\Delta n d}{\lambda}\right)\right)^2(\sin(2\varphi))^2 \qquad (1)$$

where λ is the light wavelength ($\lambda = 542$ nm) and d the sample thickness ($d = 75$ μm). The prefactor I_0 is equal to the transmitted intensity between parallel polarizers at $\varphi = 0$:

$$I_0 = I_{||}(\varphi{=}0) \qquad (2)$$

The intensity measurements are performed with an optical chopper and a lock-in amplifier from the video signal of a CCD WV-BP500 Panasonic camera from which the synchronization signal has been removed. This technique allows us to determine exactly the zone of the sample where the measurement is performed. The sample is placed into an oven, the temperature of which is controlled to within 1/100 °C. The experiments are done by raising the temperature.

In Figure 2, we report I_A as a function of φ and its best fit to eq 1. The birefringence Δn is deduced from this fit and from the I_0 measurement. The evolution of Δn as a function of temperature is shown in Figure 3. Results obtained with three different samples are reported to show the reproducibility of the experiment. From room temperature up to 34 °C, the birefringence decreases linearly; then it decreases more steeply, deviating about 10% from the low-temperarure linear law at the transition temperature (38.7 °C).

2.2. NMR Measurements. Deuterium (^{2}H) NMR gives information about motional anisotropy and is therefore sensitive to interfaces in lyotropic systems. Because of the hydration of the hydrophilic parts of the surfactant molecules, measuring the order parameter of water molecules gives information about the changes in topology of the aggregates in an ordered mesophase.[11]

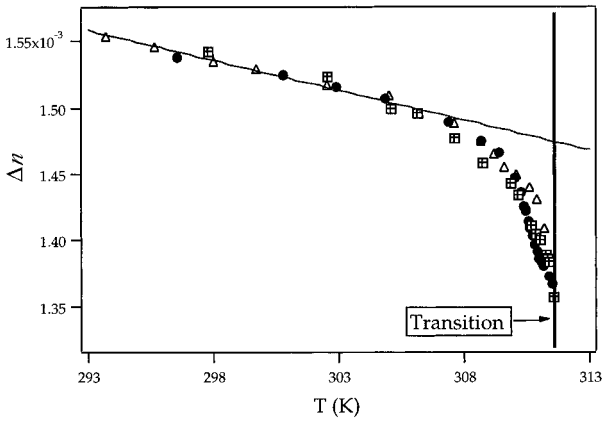

Figure 3. Birefringence Δn as a function of the temperature at the azeotropic concentration. The vertical line indicates the transition temperature. The different symbols correspond to three different samples. Error bars do not exceed symbol size.

For a deuterated water molecule undergoing anisotropic reorientational motions, the resonance spectrum is a doublet with a splitting given by

$$\Delta\nu = \nu_q \left\langle \frac{3\cos^2\theta - 1}{2} \right\rangle_t \tag{3}$$

where θ is the instantaneous angle between the O−^{2}H axis in the water molecule and the magnetic field B_0. The brackets with index t denote a time average over a time interval given by the inverse of the quadrupolar constant ν_q, i.e., 10^{-5} s. An anisotropic contribution appears only when the water molecule is bound to the surface of a cylinder. In each monodomain, the splitting may be expressed as

$$\Delta\nu = \nu_{eff} \left(\frac{3\cos^2\Omega - 1}{2} \right) \tag{4}$$

where ν_{eff} is the effective, motionally averaged quadrupolar constant of the water molecules within a monodomain. Ω is the angle between the local symmetry axis of the motions, i.e., the axis of the cylinder (optical axis) and the magnetic field B_0.

The experiments are performed on a Bruker CXP90 spectrometer with a 2 T electromagnet, operating at a ^{2}H Larmor frequency of 13 Mhz. A sample prepared with deuterated water, close to the azeotropic point, is used. The sample is placed in a sealed 5 mm tube, annealed above the transition temperature to eliminate air bubbles, and cooled extremely slowly in order to grow monodomains of a rather large size (a few 100 μm typically). However, the sample obtained in this way is not macroscopically oriented. The spectrum is then the superposition of the doublets corresponding to all possible orientations Ω of the local optical axis. It exhibits the characteristic Pake powder pattern,[12] with two dominant peaks corresponding to the 90° orientation. Such spectra in the hexagonal phase are shown in Figure 4.

Equation 4 relies on several assumptions about the motions of water molecules. First, reorientational motions occurring through the processes of hydration and diffusion of surfactant molecules on cylinders have to be fast with respect to ν_q^{-1}, i.e., faster than 10^{-5} s. The exchange time for the hydration is of the order of 10^{-11} s.[13] Then, for a cylinder diameter of the order of 30 Å and a diffusion coefficient of 10^{-11} m^2 s^{-1}, the reorientational time is of the order of 10^{-6} s. This means that a water molecule can explore the whole surface of a cylinder within the time interval ν_q^{-1}. On the other hand, the distance

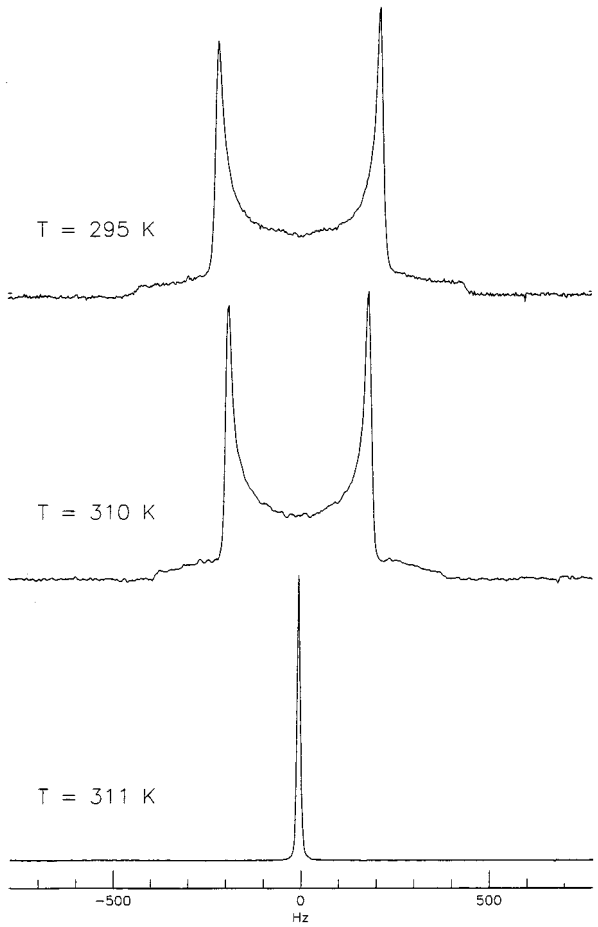

Figure 4. ^{2}H NMR spectra obtained in the hexagonal phase at T = 295 K (top) and T = 310 K (middle) and in the isotropic phase at T = 311 K (bottom), in a sample prepared with deuterated water (concentration c = 50%). The spectra in the hexagonal phase exhibit the typical Pake powder pattern.

l explored by a molecule during the relaxation of the NMR signal has to be small compared to the size of a monodomain. For a water diffusion coefficient in the hexagonal phase of the order of at most 10^{-9} m^2 s^{-1}, and a relaxation time of the order of 10 ms, the distance l is of the order of 1 μm, which is certainly much smaller than the average monodomain size. This point is confirmed by the well-resolved powder spectra which are obtained.

The splittings are determined to within 3 Hz directly on the Pake spectra. The experiments are done by raising the temperature. The temperature variation of the splitting, for a sample of concentration of 50 wt % $C_{12}EO_6$, is shown in Figure 5.

3. Interpretation

To interpret the pretransitional effect observed here, we propose that defects appear when the hexagonal/isotropic transition is approached. The structure of the fluid isotropic phase which is above the hexagonal phase is not completely understood. There is a general trend to decrease the curvature of the aggregates on increasing the temperature, because hydration of nonionic polar groups decreases with increasing temperature.[14−18] This would suggest that the fluid isotropic phase is made of disordered bilayers or branched, interconnected cylinders, rather than elongated micelles. Either the columns may spontaneously break up into shorter segments (Figure 6a) or bridges connecting close cylinders may develop (Figure 6b). In the case of fragmentation, two ends of a column are formed at each division. To avoid contact between the water and the

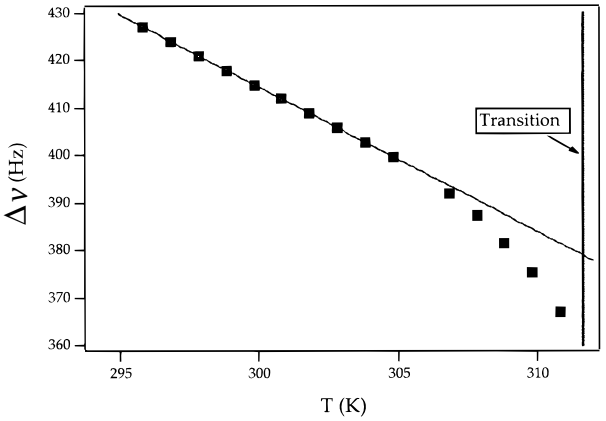

Figure 5. Temperature variation of the splitting in the hexagonal phase as a function of temperature. Error bars do not exceed symbol size.

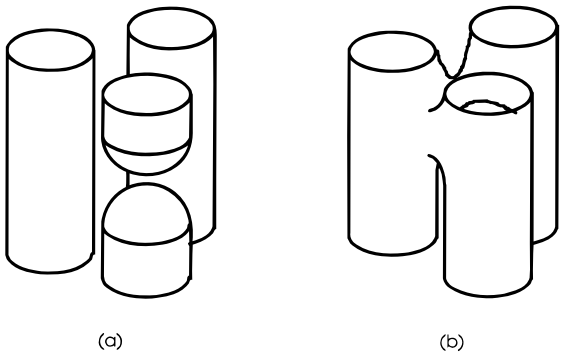

Figure 6. Schematic representation of a defect in the hexagonal phase: (a) a fragment of column ended by two spherical caps; (b) brigde connecting neighboring columns.

aliphatic chains, the interface is spherical at each extremity, which increases locally the curvature of the aggregate surface. In the second case, the curvature would locally decrease. In any case, the defects are supposed to correspond to isotropic zones, and the corresponding molecules do not contribute any longer to the birefringence, which decreases.

This effect does not explain the slow linear decrease of the birefringence at lower temperature, which we rather attribute to a regular decrease of the quadrupolar order parameter S of the molecules within the cylinders (which we suppose to be "infinite" at low enough temperature).

Another explanation could be given. Indeed, the presence of column undulations could also lead to an apparent decrease of the measured birefringence. These undulations[19] are due to a thermomechanical buckling instability, which occurs when the sample is cooled. If one is not careful, this instability can lead to easily visible stripes in planar monodomains, corresponding to a mean deviation of the column orientation, which is typically 5°. In contrast, in our experiment, stripes are hardly visible, which means that this angle is smaller. To obtain such a result, we took care to grow the sample extremely slowly in our directional solidification apparatus. Also, we waited for typically 1 day at room temperature in order to allow the thermomechanical deformation to relax to some extent. Under these conditions, the error on the measured birefringence due to cylinder undulations is negligible (less than 1% in relative value, a deviation of 5° leading to a relative decrease of Δn of the order of 2%).

Within this interpretation, it is quite easy to estimate the fraction f of molecules located in defects and their mean distance. Nevertheless, we need to further assume that the order parameter S of the molecules in the cylinders decreases linearly up to the transition temperature with the same slope as that at lower temperature. This is suggested by ESR measurements of S in the lamellar phase of the same mixture, which have shown that S decreases linearly up to the micellar transition, whereas Δn exhibits a pretransitional effect[5] as in the hexagonal phase.

We call $\alpha_{||}$ (respectively $\alpha_{\perp}$) the intrinsic polarizability of a molecule of surfactant parallel (respectively perpendicularly) to its axis and $\alpha_{||}$*) (respectively $\alpha_{\perp}$*) the mean polarizability parallel (respectively perpendicular) to the normal to the monolayer. The latter takes into account the orientational disorder of the molecule in the monolayer and depends linearly on S. Since $\alpha_{||} = \alpha_{||}$* and $\alpha_{\perp} = \alpha_{\perp}$* when $S = 1$, while $\alpha_{||}$* $= \alpha_{\perp}$* $= (\alpha_{||} + 2\alpha_{\perp})/3$ when $S = 0$, we immediately obtain

$$\alpha_{||}^* = \frac{1}{3}[(\alpha_{||} + 2\alpha_{\perp}) + 2S(\alpha_{||} - \alpha_{\perp})] \tag{5a}$$

$$\alpha_{\perp}^* = \frac{1}{3}[(\alpha_{||} + 2\alpha_{\perp}) - S(\alpha_{||} - \alpha_{\perp})] \tag{5b}$$

Now we calculate the principal polarizabilities α_i of the medium. Axis 3 is taken along the column axis (optical axis). The α_i's are obtained by taking the average of the mean polarizabilities α_{ci} of the molecules (fraction $1 - f$) belonging to straight segments of cylinder and those α_{si} of the molecules (fraction f) located in defects:

$$\alpha_i = (1 - f)\alpha_{ci} + f\alpha_{si} \tag{6}$$

with

$$\alpha_{c1} = \alpha_{c2} = \frac{\alpha_{||}^* + \alpha_{\perp}^*}{2}, \quad \alpha_{c3} = \alpha_{\perp} \tag{7}$$

$$\alpha_{s1} = \alpha_{s2} = \alpha_{s3} = \frac{\alpha_{||}^* + 2\alpha_{\perp}^*}{3} \tag{8}$$

We finally obtain

$$\alpha_1 = \alpha_2 = \frac{\alpha_{||}^* + \alpha_{\perp}^*}{2} + f\frac{\alpha_{\perp}^* - \alpha_{||}^*}{6} \tag{9a}$$

$$\alpha_3 = \alpha_{\perp}^* + f\frac{\alpha_{||}^* - \alpha_{\perp}^*}{3} \tag{9b}$$

The birefringence Δn is obtained from the Vuks relation, which relates the principal indices n_i to the principal polarizabilities:[20]

$$\frac{n_i^2 - 1}{n^2 + 2} = \frac{4\pi N\alpha_i}{3} \tag{10}$$

where N is the number of molecules per unit volume and n the mean index. Experimentally, $\Delta n \ll n$ so that the equations can be linearized. This gives, using eqs 5, 9, and 10,

$$\Delta n = \Delta n_0 S(1 - f) \tag{11}$$

where Δn_0 is a constant.

The product $\Delta n_0 S$ can be determined from a linear fit of the experimental data at low temperature (since we assume that $f = 0$ from room temperature up to $T = 34$ °C):

$$\Delta n_0 S \cong 1.647 \times 10^{-3} - 4.5 \times 10^{-6} T \tag{12}$$

where T is given in °C. If we now assume that this linear law

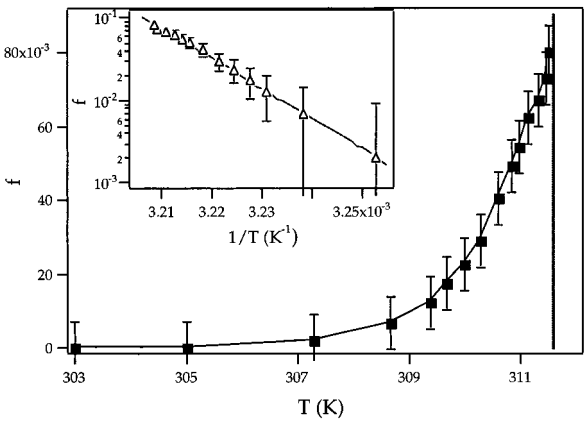

Figure 7. Fraction f of molecules belonging to column extremities (obtained from birefringence measurements) as a function of the temperature. Inset: log(f) as a function of $1/T$ (the solid line is the best fit to an Arrhenius law, eq 13).

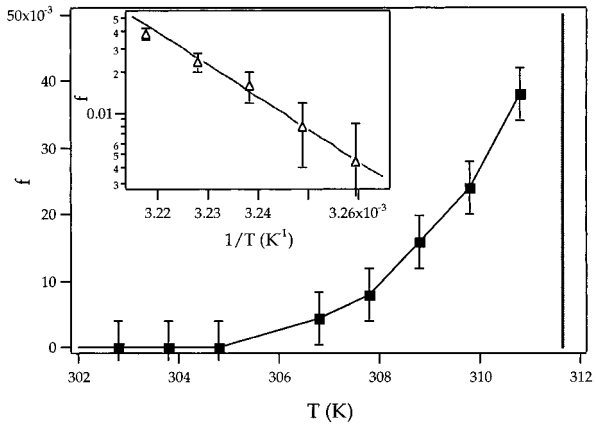

Figure 8. Fraction f of molecules belonging to column extremities (obtained from NMR measurements) as a function of temperature. Inset: log(f) as a function of $1/T$ (the solid line is the best fit to an Arrhenius law, eq 13).

is still valid from 34 °C up to the transition temperature, we can determine f by using eq 11. In Figure 7, we plotted f as a function of the temperature T. We see that f increases from 0 at 34 °C to a value of about 8% at the transition temperature. The best fit of these experimental data to an Arrhenius law

$$f = f_0 \exp\left[-\frac{E_a}{k_B}\left(\frac{1}{T} - \frac{1}{T_0}\right)\right] \tag{13}$$

where k_B is the Boltzmann constant and $T_0 \cong 311.71$ K $\equiv 38.56$ °C is the transition temperature, gives the fraction f_0 of molecules in the column ends at the transition temperature ($f_0 \cong 0.087 \pm 0.01$) and the activation energy $E_a \cong (1.16 \pm 0.3) \times 10^{-18}$ J ($\equiv 7.25 \pm 1.9$ eV), which is necessary to break a column.

The curve for the ^{2}H NMR order parameter is analyzed in the same way as that for the birefringence. The effective quadrupolar constant ν_{eff} in eq 4 is expressed as

$$\nu_{eff} = \frac{1}{2}\nu_0 SP(1 - f) \tag{14}$$

S and f are defined as before, and P is the fraction of bound water. Depending on how water molecules are bound to surfactant chains, the factor ν_0 may be actually somewhat smaller than the "bare" constant ν_q. The fraction of bound water P depends on the surfactant concentration but does not depend much on temperature.[18] P (as well as S) depends on the area per polar head, which we have assumed to be the same for all surfactant molecules throughout the aggregates. Therefore, the temperature dependence of the splitting contains the same factors as that of the birefringence. This experiment is merely a confirmation, since it does not allow us to separate the variation of S (which we assume to fall linearly with T) from that of f (due to column breaking).

As before, the linear decrease far from the transition temperature is attributed only to the variation of the order parameter, f being negligible in this temperature range, which gives

$$\nu_0 SP = 1328.6 - 3.047T \tag{15}$$

with T in °C. Again this result is in agreement with previous observations.[5,8b] Remarkably, the normalized slope of this curve $p_{\Delta\nu} \cong 3.05/1328.6 = 2.3 \times 10^{-3}$ K^{-1} is about the same (within experimental uncertainties) as that of the birefringence curve $p_{\Delta n} \cong 4.5 \times 10^{-6}/1.647 \times 10^{-3} = 2.7 \times 10^{-3}$ K^{-1}. However, this concordance may possibly be fortunate. The general trend to a decrease of the polar group hydration upon raising the temperature leads to a decrease of the curvature and relative increase of the polar group ordering perpendicular to the interfaces. Both effects lead to opposite temperature variations in the water order parameter, which are not distinguished here and may compensate to some extent. On the other end, there is a contribution in the birefringence coming from the ordering of alkyl chains, which clearly decreases with temperature.

Then, we have determined from NMR measurements the fraction f of surfactant molecules located in defects (Figure 8). At 0.8 °C below the transition, 4% of the molecules belong to column extremities. This number is comparable with the results of birefringence measurements. As shown in Figure 8, f obeys an Arrhenius law similar to eq 13 with $f_0 = 0.072 \pm 0.01$ and $E_a = 5.0 \pm 1$ eV. These values are in good accordance with those obtained in birefringence measurements.

In the following, we shall use typical values: $f_0 \cong 0.08$ and $E_a \cong 6$ eV. This latter value corresponds to an activation energy of about 0.13 eV $\cong 5k_BT$ per molecule. This order of magnitude seems reasonable, given that the energy of a hydrogen bond is close to 0.3 eV $\cong 10k_BT$.

4. Discussion

The nature of the isotropic phase is rather poorly known in the concentrated region considered here. There has been a number of studies of the isotropic phase in $C_{12}EO_y/H_2O$ systems ($y = 5-8$) in more diluted regions. There the phase is micellar, but the size and anisotropy of the micelles increase on approaching the critical line by raising the temperature or by increasing the concentration.[21−27] The critical line is thought to separate regions with small globular micelles and larger aggregates.[28] At higher concentration, some data are available, specifically temperature-jump studies of the hexagonal−isotropic transition.[29] They are probably compatible with a highly connected phase. Therefore, the exact nature of the defects, which announce the high-temperature isotropic phase, is still unclear to some extent.

We performed preliminary measurements of the diffusion coefficient of $C_{12}EO_6$ by the technique of pulsed field gradient NMR, above and below the transition, as mentionned already in a previous paper.[16] Due to the anisotropy of the hexagonal phase, the measurements lack precision in this domain. Moreover, since the phase is not macroscopically oriented, it is difficult to measure separately the diffusion coefficients $D_{\parallel}$ (parallel to the columns) and $D_{\perp}$ (perpendicular to the columns). However, the anisotropy of the diffusion ($D_{\parallel} - D_{\perp}$) may be roughly estimated. There is a consistent trend toward a strong

decrease of the diffusion anisotropy on approaching the transition. This is compatible with both models of defects. We have also measured a decrease of $D_{\|}$ close to the transition, which would be in favor of a breaking of the cylinders. However, these measurements have to be performed more extensively to be really conclusive.

The presence of defects is expected to have an effect on diffusion only if the distance L between two defects along a cylinder is comparable to, or smaller than, the typical distance over which the diffusion coefficient is measured in NMR (1 μm in practice).

We first consider the case of a fragment of cylinder terminated by two spherical caps (Figure 6a); their radius R has to be equal to 1.5 times the radius r of the cylinder($r \cong 15$ Å [1]) in order for the surface area per polar head and the volume of the aliphatic chains to remain constant.[21,30] However, we will adopt here a simplified picture in which a fragment of cylinder is terminated by a spherical cap of radius r. A denotes the surface area per polar head (which we suppose to be the same in a cylinder and in a spherical cap, $A \cong 45$ Å^2 [1]). The number of molecules contained in the cylindrical part between two cuts equals $2\pi rL/A$, while the number of molecules in the two spherical caps is $4\pi r^2/A$. So, according to the definition of f, the following relation is obtained:

$$\frac{f}{(4\pi r^2/A)} = \frac{1-f}{(2\pi rL/A)} \tag{16}$$

which gives

$$L \cong 2\frac{1-f}{f}r \tag{17}$$

With this formula and from experimental data of Figures 7 and 8, we calculate $L \cong 400$ Å at the transition temperature, while $L \cong 1$ μm when $f \cong 7 \times 10^{-3}$ i.e., typically 4 °C below the transition temperature. A spherical cap of radius $R = 1.5r$ would contain more surfactant molecules; this would lead to a larger value for L in this case (typically up to 800 Å).

We consider then the case of defects connecting cylinders. The geometry of the defects is less clear in that case. The relative area occupied by the defects is therefore more difficult to estimate. A model for cubic-like fluctuations was proposed recently, in terms of Karcher surfaces connecting cylinders three by three,[31,32] and Figure 6b is directly inspired from this model. According to ref 29 such a geometry should be more favorable in terms of curvature energy. The mesh size in the hexagonal phase is 48 Å,[8] which means that the distance between neighboring cylinders is of the order of 18 Å, i.e., comparable to the cylinder radius r. Then, the relative area of the surface within a defect is comparable to the previous case and leads to the same estimate for the average distance between defects, measured along the cylinder direction.

To conclude this section, we estimate the curvature and saddle-splay elastic constants χ and $\bar{\chi}$ of the monolayer. We use the commonly introduced quadratic form of the bending free energy density:[33]

$$g = \frac{1}{2}\chi\left(\frac{1}{R_1} + \frac{1}{R_2} - \frac{1}{r}\right)^2 + \bar{\chi}\frac{1}{R_1R_2} \tag{18}$$

where g is the free energy per unit area of monolayer, R_1 and R_2 are its principal radii of curvature, and r is its spontaneous radius of curvature in the hexagonal phase (r is the radius of a cylinder). Such a form was already introduced to describe rather concentrated systems.[34] It relies on the assumptions that direct intersurface interactions and long-range forces give weak contributions to the deformations of the aggregates which are considered here. There are some strong experimental evidences in related systems that those contributions are indeed weak compared to the bending energy variations.[35,36] We first estimate the excess of free energy of the two spherical caps formed in if a column breaks up (Figure 6a):

$$E = 2\pi(\chi + 2\bar{\chi}) \cong 6.3(\chi + 2\bar{\chi}) \tag{19}$$

Equating this energy with the activation energy E_a for f gives a first relation between χ and $\bar{\chi}$:

$$\chi + 2\bar{\chi} \cong 1.5 \times 10^{-19}\ \text{J} \tag{20}$$

Another relation is given by the measurement of the curvature constant K of the columns: $K \cong 3 \times 10^{-6}$ dyn (this value is an average of the different values given in refs 19a−c). It can be shown that bending the cylinders (radius of curvature R) costs an energy per unit volume

$$f_{\text{curvature}} = \frac{1}{2}K\frac{1}{R_2} \tag{21}$$

with[37]

$$K = \frac{\pi}{\sqrt{3}}\frac{r}{a^2}(\chi - 2\bar{\chi}) \tag{22}$$

where a is the distance between two molecular cylinders ($a =$ 45 Å) and r their radius ($r \cong 15$ Å). With this formula and $K = 3 \times 10^{-6}$ dyn, we obtain

$$\chi - 2\bar{\chi} = 2.2 \times 10^{-19}\ \text{J} \tag{23}$$

Finally, we find from eqs 20 and 23

$$\chi = 1.9 \times 10^{-19}\ \text{J} \tag{24a}$$

$$\bar{\chi} = -1.8 \times 10^{-20}\ \text{J} \tag{24b}$$

These values are comparable to those found in the litterature.[33]

In the second case (defects connecting cylinders), we suppose that the area of the defect is still on the order of $4\pi r^2$ and that the defect is constituted by a part of a minimal surface, with principal radii of curvatures r and $-r$. Then, eq 20 is replaced by

$$\chi - 2\bar{\chi} \cong 1.5 \times 10^{-19}\ \text{J} \tag{25}$$

Since eq 25 is similar to eq 23, separate values for χ and $\bar{\chi}$ cannot be estimated. Numerical values in both equations are in satisfactory agreement, given the error bars on these values. Nevertheless, it is clear that the topology of the defects is essentially determined by the sign of the gaussian curvature constant $\bar{\chi}$. A positive $\bar{\chi}$ favors the appearance of defects connecting cylinders, which have a negative gaussian curvature; inversely, a negative $\bar{\chi}$ favors the breaking of the cylinders.

In our model, the energy of a defect remains finite at the transition temperature, which means that the structure of the isotropic phase just above the transition should be reminiscent of that of the hexagonal phase. This interpretation seems to be confirmed by preliminary rheological measurements which show an "abnormal" increase of the viscosity near the transition at low shear rate.[38]

Acknowledgment. We thank J. Bechhoefer and J. F. Palierne for fruitful discussions.

References and Notes

(1) (a) Clunie, J. S.; Goodman, J. F.; Symons, P. C. *Trans. Faraday Soc*. **1969**, *65*, 287. (b) Mitchell, D. J.; Tiddy, G. J. T.; Waring, L.; Bostock, T.; McDonald, M. P. *J. Chem. Soc., Faraday Trans. 1* **1983**, *79*, 975.
(2) Allain, M. Thesis, Université Paris-Sud, Orsay, France, 1987.
(3) Paz, L.; Di Meglio J. M.; Dvolaitzky, M.; Ober, R.; Taupin C. *J. Phys. Chem.* **1988**, *88*, 3415.
(4) Allain, M. *J. Phys. (Paris)* **1985**, *46*, 225.
(5) Allain, M.; Oswald, P.; Di Méglio, J. M. *Mol. Cryst. Liq. Cryst*. **1988**, *162B*, 161.
(6) Oswald, P.; Allain, M. *J. Phys. (Paris)* **1985**, *46*, 831.
(7) Oswald, P.; Allain, M. *J. Colloid Interface Sci.* **1988**, *126*, 45.
(8) (a) Rançon, Y.; Charvolin, J. *J. Phys. Chem.* **1988**, *92*, 2646. (b) Rançon, Y.; Charvolin, J. *J. Phys. Chem*. **1988**, *92*, 6339.
(9) Oswald, P.; Moulin, M.; Metz, P.; Géminard, J. C.; Sotta, P.; Sallen, L. *J. Phys. III* **1993**, *3*, 1891.
(10) Sallen, L.; Oswald, P.; Sotta, P. To be published in *J. Phys. II.*
(11) Charvolin, J.; Hendrikx, Y. In *NMR of Liquid Crystals*; Emsley J. W., Ed.; Reidel: Dordrecht, The Netherlands, 1985.
(12) Pake, G. E. *J. Chem. Phys.* **1948**, *16*, 327.
(13) Rançon, Y. Thesis, Université Paris-Sud, Orsay, France, 1987.
(14) Israelachvili, J. N. *Intermolecular and Surface Forces*, 2nd ed.; Academic Press: London, 1992.
(15) Puvvada, S.; Blanckstein, D. *J. Chem. Phys.* **1990**, *92*, 3710.
(16) Kato, T.; Seimiya, T. *J. Phys. Chem.* **1986**, *90*, 3159.
(17) Herrington, T. M.; Sahi, S. S. *J. Colloid Interface Sci.* **1988**, *121*, 107.
(18) Nilsson, P. G.; Lindman, B. *J. Chem. Phys.* **1983**, *87*, 4756.
(19) (a) Sallen, L.; Oswald, P.; Géminard, J. C.; Malthête, J. *J. Phys. II* **1995**, *5*, 937. (b) Oswald, P.; Géminard, J. C.; Lejcek, L.; Sallen L. *J. Phys. II* **1996**, *6*, 281. (c) Clerc, M. Thesis, Université Paris-Sud, Orsay, France, 1992.
(20) Vuks, M. F. *Opt. Spektrosk*. **1966**, *60*, 644.
(21) Nilsson, P. G.; Wennerström, H.; Lindmann, B. *J. Phys. Chem.* **1983**, *87*, 1377.
(22) Brown, W.; Johnsen, R.; Stilbs, P.; Lindman, B. *J. Phys. Chem.* **1983**, *87*, 4549.
(23) Brown, W.; Rymdén, R. *J. Phys. Chem.* **1987**, *91*, 3565.
(24) Jonströmer, J.; Jönsson, B.; Lindmann, B. *J. Phys. Chem*. **1991**, *95*, 3293.
(25) Brown, W.; Zhou, P.; Rymdén, R. *J. Phys. Chem.* **1988**, *92*, 6086.
(26) Richtering, W. H.; Burchard, W.; Jahns, E.; Finkelmann, H. *J. Phys. Chem.* **1988**, *92*, 6032.
(27) Neeson, P. G.; Jennings, B. R. *Faraday Discuss. Chem. Soc*. **1983**, *76*, 353.
(28) Strey, R.; Pakusch, A. In *Proceedings of the 5th International Symposium on Surfactants*, Bordeaux, France; Mittal, K. L., Ed.; 1984; p 465.
(29) Knight, P.; Wyn-Jones, E.; Tiddy, G. J. T. *J. Phys. Chem.* **1985**, *89*, 3447.
(30) Israelachvili, J. N.; Mitchell, D. J.; Ninham, B. W. *J. Chem. Soc., Faraday Trans. 2* **1976**, *72*, 1525.
(31) Clerc, M.; Levelut, A. M.; Sadoc, J. F. *J. Phys. II* **1991**, *1*, 1263.
(32) Karcher, H. *Manuscr. Math.* **1989**, *64*, 291.
(33) Helfrich, W. in *Physics of defects*; Balian, R., Kléman, M., Poirier, J. P., Eds; North Holland: Les Houches, The Netherlands, 1980.
(34) Safran, S. A. In *Structure and Dynamics of Strongly Interacting Colloids and Supramolecular Aggregates*; Chen, S. H., et al., Eds.; Kluwer: Dordrecht, The Netherlands 1992.
(35) Gruner, S. M.; Parsegian, V. A.; Rand, R. P. *Faraday Discuss. Chem. Soc.* **1986**, *81*, 29.
(36) Vollmer, D.; Vollmer, J.; Strey, R. *Phys. Rev. E* **1996**, *54*, 3028.
(37) Oswald, P. Thesis, Université Paris-Sud, Orsay, France, 1981 (Order No. 2946).
(38) Sallen, L. Thesis, Ecole Normale Supérieure de Lyon,, France, 1996 (Order No. 23).